INTERMETALLIC PHASE GROWTH AND MICROHARDNESS OF SN42BI59 SOLDER JOINTS ON SILICON SOLAR CELLS

Derya Güldali[1,3], Angela De Rose[1], Sabine Oeser[2], Achim Kraft[1] and Ulrich Tetzlaff[3]
[1] Fraunhofer Institute for Solar Energy Systems ISE, Heidenhofstr. 2, 79110 Freiburg
[2] Fraunhofer Institute for Mechanics of Materials IWM, Wöhlerstr. 11, 79108 Freiburg
[3] Technische Hochschule Ingolstadt THI, Esplanade 10, 85049 Ingolstadt
Corresponding author: Derya Güldali, +49 (0)761 4588 2582, derya.gueldali@ise.fraunhofer.de

ABSTRACT: The temperature sensitivity of new solar cell technologies forces to use solder alloys with lower melting temperatures for interconnection [1].Our study explores the dynamics of intermetallic phase growth and microhardness in Sn42Bi58 solder joints applied to low-temperature silver metallization on silicon heterojunction (SHJ) solar cells. Through rigorous experimentation and analysis, a comprehension of the influence of these factors on the mechanical and material properties of the solder joint is achieved. Microstructural changes in Sn42Bi58 solder compared to conventional tin-lead solder are investigated through microscopy of cross sections, revealing enlarged intermetallic particles and phase boundary growth. These changes, attributed to lower homologous temperature of the low-melting solder, are expected to negatively impact the mechanical strength of the solder joint. For the intermetallic phase Ag_3Sn simulations predict a potential layer thickness of 20 µm after 25 years SHJ module operation. Our results show that the Ag_3Sn phase has a significant impact to the microhardness. Following the aging process, the nano hardness of the low-temperature Ag metallization experiences a twofold increase, shifting from 660 ± 53 N/mm² to 1367 ± 411 N/mm². This strengthening is primarily attributed to the prevailing influence of the Ag_3Sn intermetallic phase.
Keywords: Lead-free soldering, intermetallic compounds, microhardness, interconnection, long-term stability

1 INTRODUCTION

Research on low-temperature soldering is important to realize the industrialization of lead-free Photovoltaic-modules (PV modules) and the interconnection of temperature sensitive high efficiency cell technologies (*e.g.*, tandem solar cells). Both will be highly relevant for the PV industry in the near future. The progress in solar cell architecture to more efficient solar cells [2] leads to an adaptation of the conventional backend processes (*i.e.,* metallization and interconnection) in PV module manufacturing as the maximum soldering temperature has to be reduced to avoid damaging the solar cells. In turns, this means switching to alternative solder alloys with a lower melting point than the current standard Sn60Pb40 with $T_m \approx$ 183-190 °C.

However, due to the fact that PV is still excluded from the current European RoHS (Restriction of Hazardous Substances) regulations [3], Pb-containing solder is still dominant due to its good performance and low price. For general low-temperature (LT) soldering processes as *e.g.,* in microelectronics, several LT solder alloys could be used. For soldering in PV, the restrictions (*i.e.,* material compatibility with solar cell, long-term stability, costs etc.) drastically reduce the possible choice of LT alloy. To lower the melting point and to decrease the soldering temperature, either one of the elements Sn, In, Bi or Ga has to be used [4]. In PV, the most well-known low-melting solder alloy is the eutectic tin-bismuth alloy (Sn42Bi58). It has been under investigation by research and industry in the past decades [5–8].

SnBi solder has some advantages in terms of processability (relevant physical properties *e.g.*, melting point) and human and environmental acceptability (*e.g.*, toxicity). A comparison of the conventional tin-lead solder with the lead-free alternative regarding the most relevant criteria for low-temperature soldering is shown in Figure 1. The dominant solder alloy of current PV modules Sn60Pb40 contains 40 $\%_{wt}$ lead, which sums up to about 8-10 g/m² lead per full-size solar module [9, 10]. Lead is considered hazardous to health and environment and is included in the category of RoHS-restricted materials for electrical and electronic equipment [3]. In fact, it is only a question of time until this restriction will also cover PV products so that Sn60Pb40 has to be substituted by alternative Pb-free solder alloys. In general, Sn42Bi58 has no known harmful properties compared to Sn60Pb40 solder, making it friendlier to the environment and health. Compared to tin-lead solder, bismuth-based alloys have a lower electrical conductivity and a higher tendency for oxidation during soldering, which leads to reduced wettability. Sn42Bi58 is a promising and cost-effective alternative solder alloy for the industry, but research in this area is not yet complete and more understanding is needed in terms of fundamentals and long-term behavior of the solder.

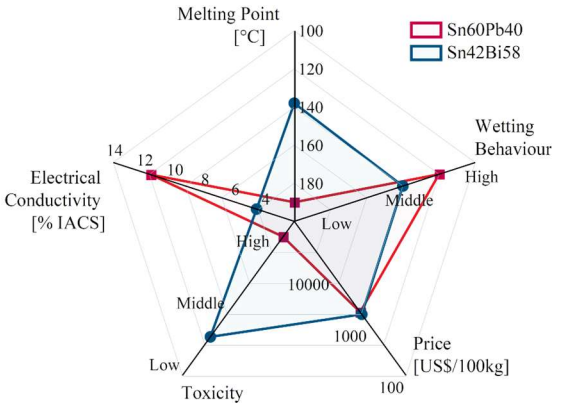

Figure 1: Overview of important criteria (melting point, electrical conductivity according to IACS, toxicity, price and wetting behavior) for the application of the most prominent solder alloys in PV: Sn60Pb40 and the lead-free alternative Sn42Bi58. The further out the alloy is located on the respective axis, the more suitable it is for low-temperature interconnection for Si solar cells. Data taken from [11–15].

2 THEORETICAL BACKROUND

2.1 Solder joint of silicon solar cells

Solder joints of Si solar cells have an important task as they mechanically and electrically contact the cell's electrodes for collection of the generated current. This is achieved by establishing a reliable connection between the

cell ribbon and the metallization of the solar cell (see Figure 2).

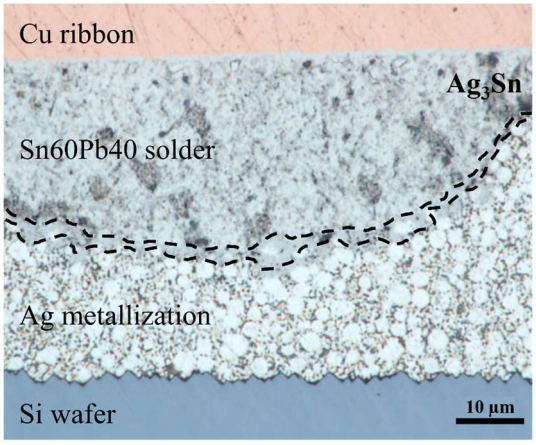

Figure 2: Microscopic image (cross section) showing the solder joint with Sn60Pb40 solder and Cu-ribbon on LT Ag metallization of an SHJ solar cell. The formation of the intermetallic phase Ag_3Sn (highlighted by black dashed line) implies successful wetting and solder joint formation.

To achieve a large contacted area between solder and metallization, sufficient and continuous wetting of the busbars by the solder is necessary (see chapter 2.2). Additionally, the proportion of non-electrically conductive areas, such as cracks and voids (*e.g.*, air inclusions), should be minimized. Considering that the module is subjected to various thermomechanical and mechanical stresses, the solder joint should exhibit stability against these loads.

The quality and design of solder joints have a significant impact on several aspects, including mechanical stress during string production, transport of the electric current of photoconversion and long-term stability of the photovoltaic module. Cases of coarsening of the solder and fatigue cracks in the solder joint have been reported for photovoltaic modules that have been exposed to outdoor conditions for an extended period of time [16, 17].

Therefore, fundamental understanding of solder joints as well as detailed analysis is evident to evaluate modifications such as the solder coating of the ribbons, in order to ensure the continued stability of the solder joints.

2.2 Intermetallic compounds

As mentioned in chapter 2.1, contact formation between the cell ribbon and the busbar is essential for the power output of the PV module. This process is known as joining. According to DIN 8580, this involves the joining of two or more components or materials (here: cell ribbon and metallization) with a formless solid (here: solder) [18].

In PV, mostly infrared soldering is used with solder-coated Cu ribbons (see Figure 2). Due to the soldering temperatures during the process, atomic exchange processes lead to interatomic diffusion at the interfaces between Cu ribbon and solder and between solder and metallization, resulting in the formation of diffusion zones. As a result, solid solutions and/or intermetallic compounds/phases (IMC) can form at this interface. The formation of these phases depends on factors such as the mutual solubility of the materials, the crystal structures of the materials to be joined and the temperatures prevailing during the soldering and the subsequent cooling process. The existence of a diffusion zone is a prerequisite for forming a reliable electrical contact.

When joining Sn- and Ag-containing components, an IMC of Sn-Ag-phases is formed at the interface. According to the binary phase diagram (see Figure 3), this phase consists of 75 $\%_{at}$ Ag and 25 $\%_{at}$ Sn (Ag_3Sn) and is stable at room temperature. On conventional Si solar cells, this phase can be found at the interface between the Ag metallization and the Sn-containing solder (see Figure 4).

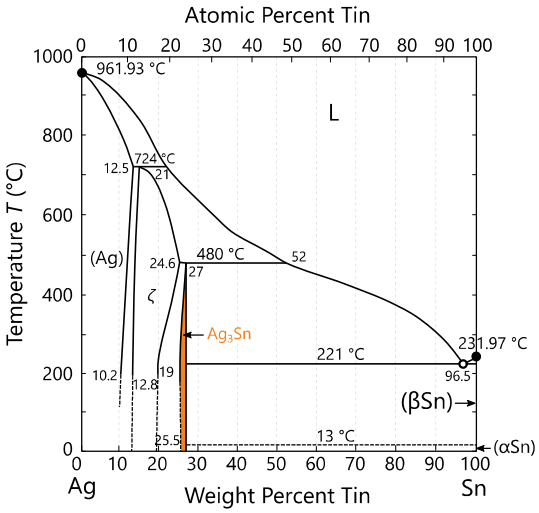

Figure 3: Binary tin-silver phase diagram. The intermetallic phase Ag_3Sn is highlighted in orange. Adopted from [11].

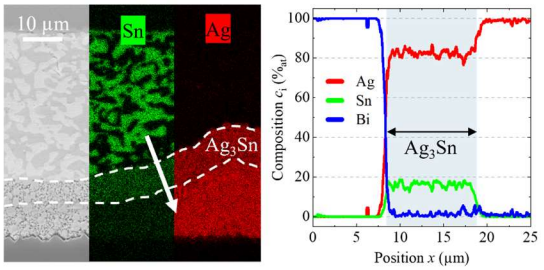

Figure 4: Analysis to identify Ag_3Sn in the solder joint, shown for a lead-free joint. Left: SEM image and EDX mapping of the solder joint. Right: EDX line scan across the interface solder/metallization.

With this intermetallic phase being part of the solder joint, the mechanical as well as electrical properties of the joint change. When the solder joint is in operation and exposed to various environmental influences (*e.g.*, high outdoor temperatures and temperature changes), a change in the microstructure of the solder joints is expected, which consequently changes the properties of the solder joint. The thickness as well as hardness of the IMC is an important parameter for the quality of the whole solder joint. The growth behavior of various IMC under isothermal aging has already attracted much attention in other electronic fields [19, 20] as well as in PV [5, 21–24]. Studies have also shown that the failure mechanisms of solder joints are often associated with the presence and growth of intermetallic compounds at the substrate-solder interface [25–27]. IMCs often exhibit very high hardness and lower electrical conductivity due to their complex crystal structure, among other factors. As a result, an increase of the thickness of this layer would lead to

embrittlement of the solder joint and crack initiation or propagation.

The understanding of the microstructure of the solder joint and especially of the IMC as well as its effect on the stability of PV modules is currently not entirely developed and needs more investigations.

2.3 Modelling the growth characteristics of IMCs

In the joint of the solar cell, there is a special solid-state diffusion process between the Sn in the solder and the Ag in a metallization. Since it is not a pure metal-metal diffusion, describing this diffusion is complex. Therefore, for the subsequent calculations, a simple approximation with a known solution of Fick's law is chosen in the first step. This approach has already been used in other studies investigating intermetallic phase growth [23, 26, 28].

The growth behavior of the intermetallic layer Ag_3Sn during solid state aging can be described by the diffusion of Sn and Ag atoms to each other. As the thickness of the IMC layer increases over time, the flux of atoms during diffusion decreases. This behavior can be represented by the parabolic time law (Eq. 1). The equation can be interpreted as a special one-dimensional solution of the second Fick's law, where x^2 is defined as the mean square diffusion distance of the atoms over the time t [29]. For all following calculations, it is assumed that the root of the mean square diffusion distance x^2 is equal to the intermetallic layer thickness x. By transforming the equation, the obtained relationship for the thickness x of the intermetallic phase is achieved:

$$x^2 = 2Dt \qquad \text{Eq. 1}$$

$$x = \sqrt{2Dt} \qquad \text{Eq. 2}$$

The Arrhenius relationship, given in Eq. 3, describes the temperature-dependent behavior of the diffusion coefficient D in materials [29, 30]. It states that the diffusion coefficient is exponentially proportional to the reciprocal of temperature T, where an increase in temperature leads to an acceleration of diffusion processes:

$$D = D_0 e^{-\frac{Q}{RT}} \qquad \text{Eq. 3}$$

The equation involves the diffusion constant as a thermally independent constant D_0, activation energy Q, the gas constant R and the absolute temperature T as components, expressing the temperature dependence of diffusion behavior. D_0 and Q are material-specific constants, both depending on the considered diffusion mechanism and system. Combining Eqs. 2 and 3 leads to Eq. 4:

$$x = \sqrt{2\, D_0 e^{-\frac{Q}{RT}}\, t} \qquad \text{Eq. 4}$$

To determine the activation energy Q, the Eq. 4 is linearized through the application of the natural logarithm, leading to the formulation of Eq. 5:

$$\ln(x) = \frac{1}{2}\ln(2D_0 t) - \frac{Q}{2R}\frac{1}{T} \qquad \text{Eq. 5}$$

By simplifying the function $\ln(x)$ with respect to $1/T$, a linear relationship between Q and R is obtained, which is characterized by the slope labeled "a":

$$Q = -2aR \qquad \text{Eq. 6}$$

There are two possible approaches for calculating the diffusion constant D_0: For the first option, the relation $\ln x$ and $1/T$ is used as already done for the calculation of the activation energy (Eq. 6).

The second approach uses the Eq. 2 and the relation $x \sim t^{1/2}$. The slope a_* of this equation allows to calculate the diffusion coefficient, resulting in the diffusion constant using the Arrhenius relationship (Eq. 3):

$$D_0 = \frac{D}{e^{-\frac{Q}{RT}}} = \frac{a_*^2}{e^{-\frac{Q}{RT}}} \qquad \text{Eq. 7}$$

Since the first approach generates a large error, the second approach (Eq. 7) is used for the calculations in this work.

Utilizing these two quantities, it becomes possible to forecast the increase in layer thicknesses at various temperatures and durations as by Eq. 4. This equation can also be employed to infer aging parameters, including time and temperature, to achieve a specific layer thickness:

$$t = \frac{x^2}{2 \cdot D_0 \cdot e^{-\frac{Q}{RT}}} \qquad \text{Eq. 8}$$

$$T = \frac{Q}{R} \cdot \frac{1}{\ln(D_0 t) - 2\ln(x)} \qquad \text{Eq. 9}$$

These calculations allow to estimate the growth of the Ag_3Sn intermetallic phase and to investigate the relevance of the influence of the phase on the module stability. The aim is to predict the changes of critical phases in the solder joint between Cu ribbon and solar cell over the lifetime of a PV module and to study its impact.

3 MATERIALS AND METHODS

3.1 Materials

Using a screen-printing process, the metallization is realized at Fraunhofer ISE PV-TEC laboratory in a five busbar (BB) layout on the front and rear side, with a constant BB width of 0.8 mm on industrial silicon heterojunction wafer (M6, n-type, Cz-Si, textured, bifacial). Table 1 lists the cell ribbons used for the interconnection of the SHJ solar cells.

Table I: Compilation of the used cell ribbons with their respective geometric and material-specific properties.

Leaded Solder (Reference)
Cu ribbon (0.90 × 0.22 mm²) coated with 20-25 µm **Sn60Pb40** (near-eutectic, T_m: 183-190 °C)
Lead-Free Solder
Cu ribbon (0.90 × 0.22 mm²) coated with 15-25 µm **Sn42Bi58** (eutectic, T_m: 139 °C)

3.2 Solar cell interconnection

Soldering is realized on a manual laboratory setup to be more flexible for process parameter and material variations. We used manual soldering with a solder iron supported by heating plates for preheating of the solar cells, using the following set-temperatures:

- Sn60Pb40: Preheating 120 °C, Soldering 240 °C
- Sn42Bi58: Preheating 100 °C, Soldering 180 °C

Prior to soldering, a conventional no-clean flux with a low solid content is applied locally to the solar cell busbars to facilitate the reduction of oxides and support wetting.

3.3 Metallography

For the evaluation of the solder joint microstructure, metallographic cross sections are prepared out of the soldered SHJ solar cells. After laser cutting of small pieces along the soldered busbar, the samples are embedded into epoxy resin and polished perpendicular to the cross section of the Cu ribbon.

3.4 Isothermal aging

To comprehend the metallurgical behavior within the solder joints, we conduct isothermal aging experiments to assess how microstructural changes evolve concerning temperature and time. The aging process is conducted in an atmospheric air-drying oven, exposing prepared samples to aging at 65 °C, 85 °C, 105 °C and 125 °C for a total duration of 168 hours (7 days). Isothermal aging is performed similarly to the standard DIN EN 60068-2-2, a norm for a dry heat test method [31]. Optical microscopy images are captured in the initial state and at specific time intervals (24 h, 96 h, 168 h).

3.5 Characterization of microstructure

Both scanning electron microscopy (SEM) and energy diffractive X-ray (EDX) spectroscopy are employed to analyze the samples in their initial state and after 168 hours. These techniques provide comprehensive insights into diffusion zones and IMC formation at the joints' interfaces.

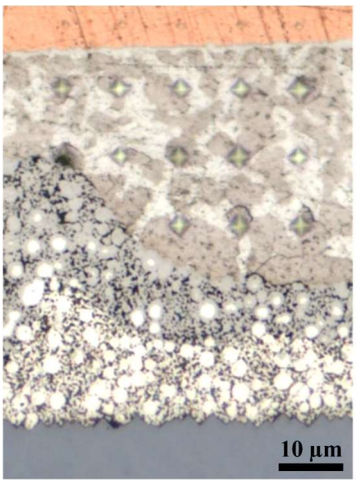

Figure 5: Optical microscope image of a solder joint (cross section view) after hardness measurement using nanoindentation [32]. The hardness indentations of the Berkovich pyramid in the solder are clearly visible. Due to the higher hardness of the other solder joint components, the indents in the Cu ribbon, the Ag metallization and the Si wafer are hard to identify in the image.

Resulting images will provide the basis for thickness measurements of the IMC for the calculation of the growth parameters given in chapter 2.3. In addition, an instrumented indentation test in the nano range according to DIN EN ISO 14577-1 [32] is employed to determine the microhardness in the solder joint. The hardness measurements were performed at Fraunhofer Institute for Mechanics of Materials (IWM). Multiple indentations are created per cross section sample using a standardized Berkovich diamond tip with an applied force of 2 mN and a dwell time of 10 s to ascertain the hardness values. To achieve this, a grid (50 × 70 µm) with 5 × 9 indentations was defined to cover each phase within the solder joint (see example in Figure 5).

4 RESULTS AND DISCUSSION

4.1 Evaluation of microstructural changes after isothermal aging

As grain coarsening and IMC growth primarily result from diffusion processes, which are significantly temperature-dependent, it's reasonable to investigate these phenomena exclusively through isothermal aging experiments. External factors like humidity are negligible and have no impact on the quantitative outcomes of our study. Specifically, comprehending the growth kinetics of IMCs and deriving practically applicable model parameters necessitates systematic aging experiments conducted at various isothermal temperature.

At each time interval and at specific aging temperatures, the thickness of the IMC layer is measured using an optical microscope. In Figure 6, the resulting IMC layer thickness x, determined by 20 measurements per cross section, is plotted against the square root of time $t^{1/2}$. Note that the chosen approach from Eq. 2 correlates well with the results. A linear regression is necessary to read out the y-axis intercept c according to Eq. 7, the diffusion constants D_0 for the Ag_3Sn phase can then be calculated using "c".

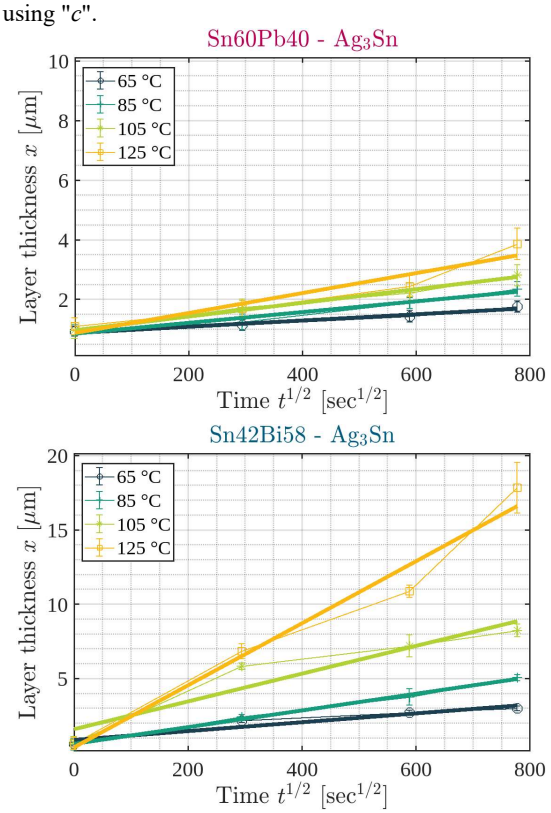

Figure 6: The plots represent the growth of the Ag_3Sn phase in the bismuth-containing (top) and lead-containing (bottom) solder joints and the linear fit of each temperature. The layer thickness x is plotted over the square root of time $t^{1/2}$. Note that different scaling is applied to each diagram for clarity.

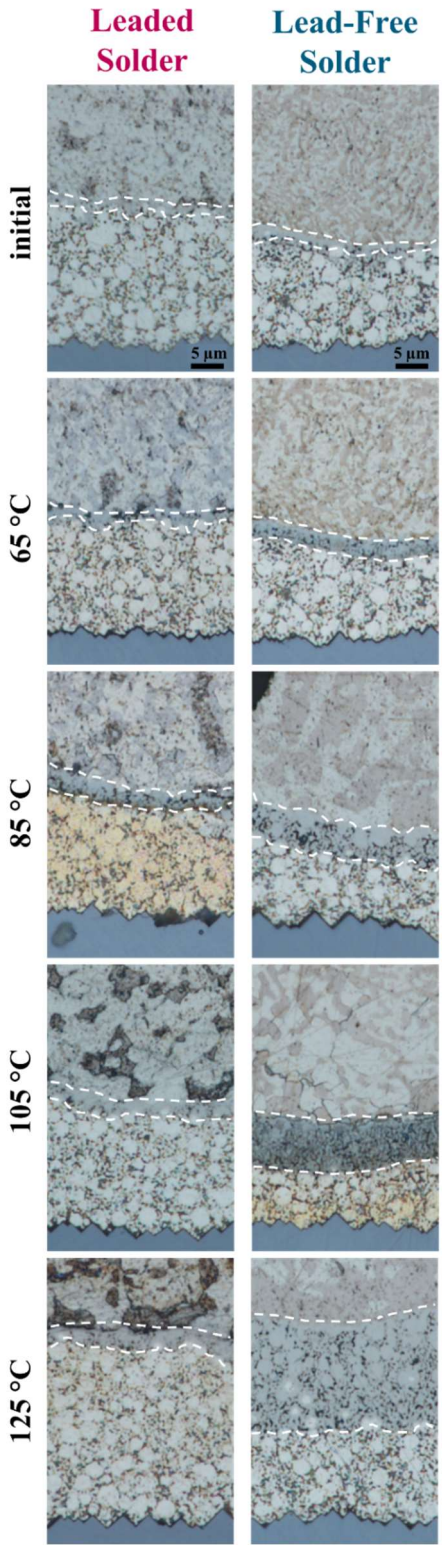

Figure 7: Microscopic images (cross sections) showing joints on SHJ solar cells with soldered ribbons (blue: lead-free solder, red: leaded solder) in the initial state, at 65 °C, 85 °C, 105 °C and 125 °C after 168 h aging in atmospheric air. After aging, the intermetallic phase Ag_3Sn (in white) grows into the Ag metallization, which is a consequence of the diffusion of Sn from Sn42Bi58 and Sn60Pb40 solder.

The analysis of the cross section by microscopy reveals a different microstructure and aging behavior of Bi-containing solder joints compared to conventional Pb-containing solder joints (see Figure 7). For both, Sn diffusion into the Ag metallization is observed, forming the IMC Ag_3Sn at the interface. Due to the lower melting point of SnBi and an increased atom mobility within the crystal lattice, the Sn diffusion is more pronounced within the SnBi solder joint [33–36]. The Sn atoms at the interface diffuse into the metallization to form the Ag_3Sn phase. As a result, the Bi-rich phases remaining at the interface come together to form larger grains, similar to the process of Ostwald ripening [35].The closer the aging temperature to the melting point of the respective solder alloy, the stronger becomes the diffusion velocities in the crystal lattice due to the increasing homologous temperature.

The plots in Figure 8 show the natural logarithm of the Ag_3Sn layer thickness x plotted against $1/T$ for the three different aging times. From the arithmetic mean of the three fits, the activation energy Q can be determined in accordance with Eq. 6. from whose slope a and intercept c (intersection with y-axis), the activation energy Q can be determined in analogy to Eq. 6.

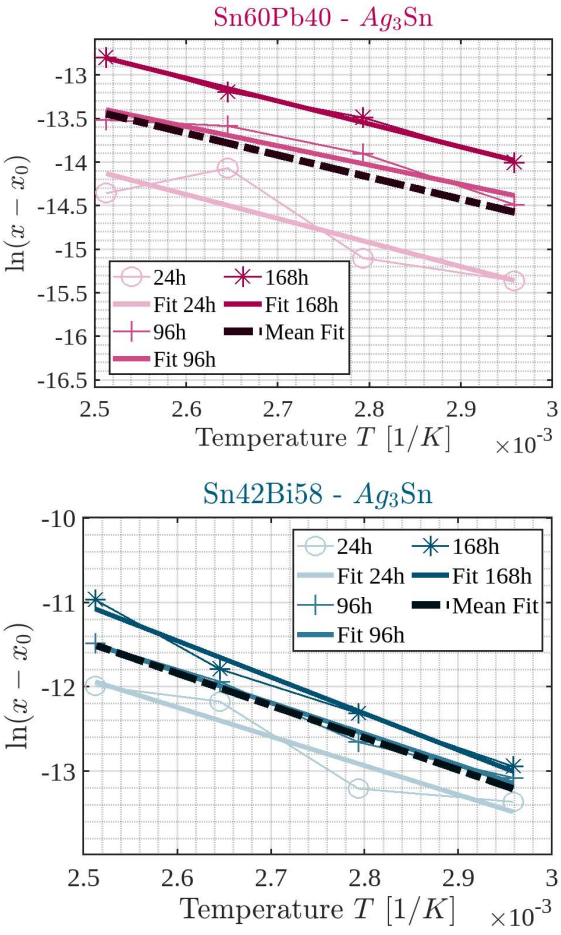

Figure 8: Arrhenius plots of Ag_3Sn IMC growth in both solder alloys for different aging times. The natural logarithm of IMC phase thickness $\ln(x\text{-}x_0)$ is plotted over the inverse of the temperature $1/T$.

As explained in chapter 2.3, the diffusion constant D_0 is calculated using the slope a of the diagrams in Figure 6.

The mean value of all 4 temperature graphs is calculated and listed in Table II.

Table II: Activation energies Q and diffusion coefficients D_0 resulting from the slope and the ordinate intercept of the data plotted in Figure 7, using Equations 6 & 7.

Solder alloy	Q [kJ/mol]	D_0 [m²/s]
Sn60Pb40	42.1 ± 4.8	$(1.9 \pm 0.2) \times 10^{-12}$
Sn42Bi58	63.5 ± 7.4	$(3.3 \pm 1.0) \times 10^{-8}$

The calculated values for Q and D_0 clearly illustrate why there is a stronger growth of the Ag_3Sn phase in the Sn42Bi58 solder. With increasing temperature, a higher activation energy leads to a steeper rise in the diffusion coefficient D, considering the Arrhenius relationship from Eq. 3. Furthermore, from the comparison of the activation energy of the two solders, it can be interpreted that there is a correlation with the Sn content in the solder. The lead-containing solder has a higher Sn content (60 $\%_{wt}$) in comparison to the bismuth-containing solder (42 $\%_{wt}$). Since only Sn contributes to the formation of the Ag_3Sn phase, it is logical that a higher Sn content in the solder lowers the energy barrier for the formation of this intermetallic phase, as more Sn is available for diffusion [26]. However, the Sn60Pb40 solder still exhibits slower phase growth, as its homologous temperature (for 125 °C: Sn60Pb40 0.87-0.89 and Sn42Bi58 0.97) is higher than that of the lead-free, low-temperature solder. This factor also significantly influences the growth rate. Based on the measured layer thicknesses and the resulting calculated material properties, a trend towards almost 5-fold stronger growth of the intermetallic phase in the Sn42Bi58 solder on this low-temperature metallization can be observed.

For both solder alloys, a growth of the Ag_3Sn phase is observed, which is driven by the segregation of the base materials. This process is based on the effort to reduce the total energy in the system and to establish an equilibrium [37]. Looking into the alloy phase diagrams (not shown here), it is obvious that the respective elements have a very low solubility (for the temperature range used here) in each other, resulting in precipitates/phases which subsequently agglomerate into lager grains to reduce the surface energy. As a result, the increase of Bi-rich grains can lead to a reduction in fatigue strength, ending in a lower resilience to mechanical stress, during the lifetime of photovoltaic modules. Additionally, the dominance of grain coarsening as a failure mode in solder joints was a significant reliability issue in electronics [38, 39]]. This phenomenon was clearly associated with fatigue cracking in PV modules after extended outdoor exposure [16, 40–42].

4.2 Modeling of Ag_3Sn intermetallic phase growth

Utilizing these material attributes, it becomes feasible to predict the phase growth under the specified reliability test conditions, which are commonly employed for the certification of PV modules. An established and important test for heat exposure is the damp heat test according to IEC 61215:2021 [43]. For 1000 h, the specimens are aged in the simulation at a constant temperature of 85 °C under 85 % relative humidity. Based on Eq. 4, the calculated results are shown in Figure 9, illustrating that the Ag_3Sn phase in low-melting solders, such as Sn42Bi58, is expected to grow excessively up to 12 µm layer thickness x after 1000 h at 85 °C. Note that the influence of the humidity is neglected here. Based on the calculated material parameters, the leaded solder joint would reach a thickness of about 4 µm after 1000 h damp heat test, ~1/3 of the phase thickness in the lead-free solder. It should be noted that in the simulations, there is no upper limit for the layer thickness of intermetallic phases. However, under real conditions, growth is constrained by the thickness of the metallization. Additionally, the depletion of Sn in the solder layer also leads to a slowdown of Sn diffusion towards the Ag metallization.

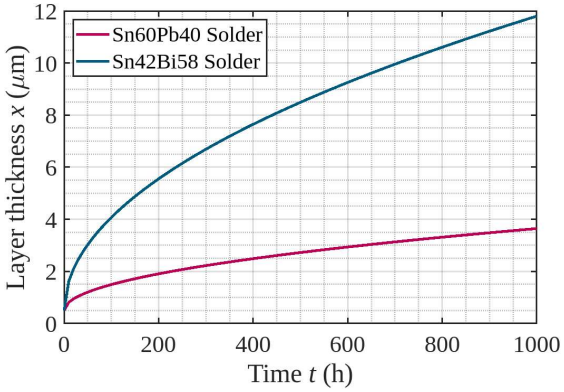

Figure 9: Simulated phase growth of Ag_3Sn over a duration of 1000 hours at 85 °C, reproducing the temperature conditions of the damp heat tests as defined in IEC 61215:2021 [43].

Usually, manufacturers provide a 25-year warranty on their PV modules. Using the numerical simulations and the corresponding calculations, the growth of the Ag_3Sn phase in LT metallization over 25 years was determined (see Figure 10). For this purpose, an annual average ambient temperature in Germany of 10.5 °C (2022) [44] and an initial layer thickness of x_0 = 0.5 µm after interconnection are assumed. It turns out that the IMC reaches a layer thickness of ~ 11 µm for the low-melting solder (blue line in Figure 10). The thickness for the conventional tin-lead solder is ~ 7.8 µm.

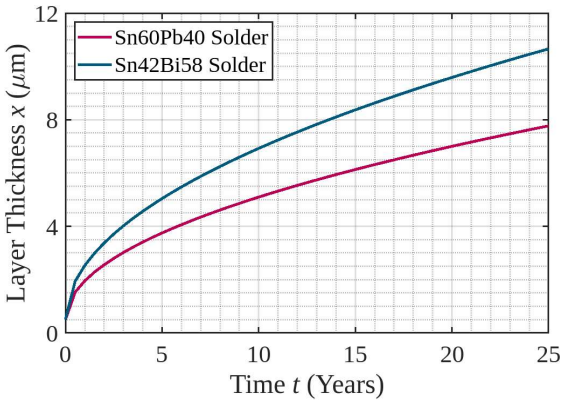

Figure 10: Simulated phase growth of Ag_3Sn over a duration of 25 years at 10.5 °C with an initial layer thickness of x_0 = 0.5 µm.

Nevertheless, the simulation misses validation by comparison with experimentally measured IMC growth after long-term exposure to humid heat, thermal cycling or extended outdoor conditions, which will be addressed in future work. The simulations help to understand and predict the behavior of intermetallic phase growth in LT Ag metallization, as it is used for SHJ or perovskite Si tandem solar cells. It is important to mention that the

calculated characteristic values for the activation energy Q and diffusion constant D_0 are valid for this joining system. Changes in the metallization paste lead to changes in the diffusion process, including the presence of more or less vacancies and diffusion paths, which would accelerate or slow down Sn diffusion.

4.3 Effect of IMC growth on microhardness

The clear Ag_3Sn phase growth influences the microstructure of the solder joint. Beside electrical changes, this causes an increase in microhardness in particular regions. Figure 11 shows the Martens hardness HM plotted against the position within the solder joint for the initial state (top) and after isothermal aging at 125 °C for 168 h (bottom). Post aging, the hardness of the Ag metallization witnesses a 2-fold rise, increasing from 660 ± 53 N/mm² to 1367 ± 411 N/mm², with the presence of the Ag_3Sn intermetallic phase predominantly influencing this enhancement. Similarly, the hardness of the Ag_3Sn phase in the lead-containing solder displays comparability at 1366 ± 237 N/mm² (not shown here). The hardness of the other components (Si wafer, pure Ag metallization, solder and Cu ribbon) is only slightly affected by the temperature exposure The hardness of the other components (Si wafer, pure Ag metallization, solder and Cu ribbon) is only slightly affected by the temperature exposure.

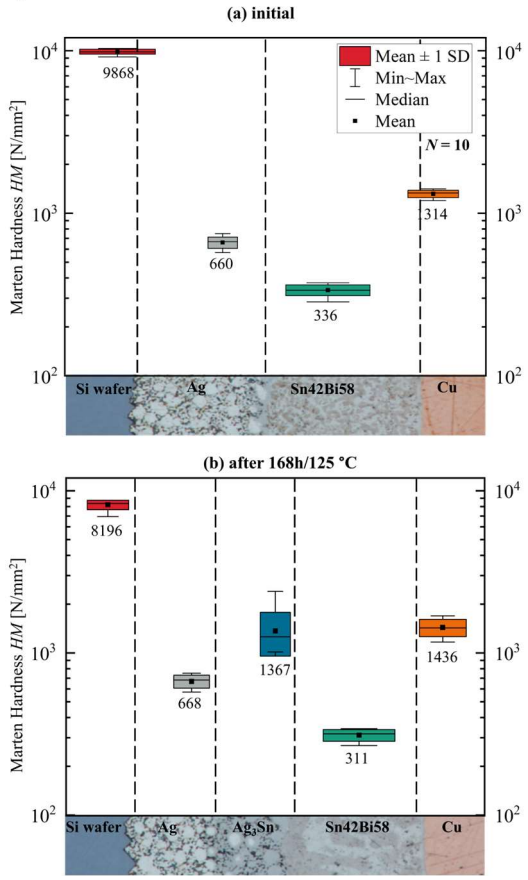

Figure 11: Distribution of microhardness in the solder joint of the eutectic bismuth-tin solder measured by nanoindentation [32] in the initial state and after 168 h at a constant aging temperature of 125 °C in atmospheric air (10 measurements values per group). The effect of the observed high growth of the intermetallic phase Ag_3Sn in Figure 5 is reflected here in the increase in hardness within the Ag metallization.

However, the significant expansion of the IMC in the Bi solder joint indicates that due to the lower homologous temperature, the overall solder joint hardness grows progressively over time. During temperature cycling, these components with significantly higher hardness than the surrounding materials, can lead to thermal stress during temperature cycling. This thermal stress can result in solder joint cracking or detachment, especially if the thermal expansion coefficients of the materials are mismatched. The higher hardness of the IMC can be more prone to brittle fracture, especially if the solder joint experiences rapid temperature changes during day-night cycle or mechanical loading by *e.g.,* snow. Brittle fractures can lead to solder joint failure [39, 45]. Consequently, the occurrence of a joint crack could lead to elevated series resistances and a subsequent reduction in current delivery.

5 CONCLUSIONS AND OUTLOOK

In conclusion, this study explored intermetallic phase growth and microhardness in Sn42Bi58 solder joints on silicon heterojunction solar cells. Through rigorous experimentation and analysis, we gained a comprehensive understanding of how these factors affect solder joint mechanical and material properties.

Microstructural changes, observed through microscopy, revealed significant alterations in the Sn42Bi58 solder matrix compared to traditional tin-lead solder. These changes included thicker Ag_3Sn intermetallic compound layers and increased grain boundary growth between phases, potentially compromising solder joint mechanical strength. Simulations, based on an upper limit scenario, indicated that this could lead to a layer thickness of approximately 11 µm over 25 years at 10.5°C. These microstructural variations also influenced microhardness, with an observable increase from 660 N/mm² to 1367 N/mm², primarily due to the Ag_3Sn phase.

Comparing these two solder compositions highlighted distinct kinetics and behaviors of intermetallic phases. The prevalence of the Ag3Sn phase in Sn42Bi58 solder joints on low-temperature Ag metallization emphasized its potential impact on joint mechanical properties. The interplay between intermetallic compounds and different solder materials offered insights for optimizing solder joint reliability and performance in various applications.

These findings provide a foundation for enhancing soldering processes and material selection across industries. Further exploration is needed to understand the effects of intermetallic layer growth, either alongside or compared to grain coarsening in the solder matrix. This exploration should include failure analysis of field-aged PV modules and correlating IMC growth with solder joint mechanical properties.

Moreover, comprehensive understanding of processes and materials, along with stringent control, is vital to establish meaningful correlations between simulation and experimentation. Our simulation results serve as comprehensive predictions within the given conditions.

This study underscores the importance of intermetallic phases in solder joint behavior, particularly their role in governing microhardness and, consequently, the overall structural integrity of solar cell assemblies. These insights offer valuable groundwork for enhancing photovoltaic module reliability and performance, contributing to advancements in solar energy technology. The study focused on Sn42Bi58 solder on low-temperature

metallization. Future research should investigate whether other low-temperature solders exhibit similar behavior. Our findings suggest that the growth of the brittle Ag3Sn phase depends on factors like solder homologous temperature, Sn content, element solubility, and metallization characteristics. Low-temperature solders with different properties may have different phase growth behaviors, emphasizing the complexity of solder joint behavior and the need for comprehensive analysis.

ACKNOWLEDGEMENTS

This work was supported by the German Federal Ministry for Economic Affairs and Climate Action within the project Utility4Indium (contract no. 020E-100487483).

REFERENCES

[1] B. A. Korevaar, J. A. Fronheiser, X. Zhang, L. M. Fedor, and T. R. Tolliver, "Influence of annealing on performance for hetero-junction a-Si/c-Si devices," in *Proceedings of the 23rd European Photovoltaic Solar Energy Conference and Exhibition*, Valencia, Spain, 2008, pp. 1859–1862.

[2] ITRPV, "International Technology Roadmap for Photovoltaic (ITRPV): 2022 Results," 2023.

[3] *RoHS-Richtlinie 2011/65/EU: Beschränkung der Verwendung bestimmter gefährlicher Stoffe in Elektro- und Elektronikgeräten*, 2011.

[4] G. Humpston and D. M. Jacobson, *Principles of soldering*. Materials Park, Ohio: ASM International, 2004.

[5] T. Geipel, M. Moeller, J. Walter, A. Kraft, and U. Eitner, "Intermetallic compounds in solar cell interconnections: Microstructure and growth kinetics," *Sol Energ Mat Sol C*, vol. 159, pp. 370–388, 2017, doi: 10.1016/j.solmat.2016.08.039.

[6] B. Lalaguna, P. Sánchez-Friera, I. J. Bennett, D. Sánchez, L. J. Caballero, and Alonso J., "Evaluation of bismuth-based solder alloys for low-stress interconnection of industrial crystalline silicon PV cells," in *Proceedings of the 22nd European Photovoltaic Solar Energy Conference and Exhibition (EUPVSEC)*, Milan, Italy, 2007, pp. 2712–2715.

[7] M. Nowottnick and A. Novikov, "Possibilities and Limits of Bismuth Solders," in *Proc. of SMTA International*, Rosemont, USA, 2017, pp. 195–200.

[8] D. Güldali and A. De Rose, "Material Joint Analysis of Lead-Free Interconnection Technologies for Silicon Photovoltaics," in *45th International Spring Seminar on Electronics Technology (ISSE)*, 2022.

[9] Paul Gebhardt *et al.,* "Lead-Free PV Modules: Industrial Realization and Evaluation of Environmental Impact," in *8th World Conference on Photovoltaic Energy Conversion*, Milano, 2022, pp. 930–934.

[10] Dr. Harry Wirth | Fraunhofer ISE, "Recent Facts about Photovoltaics in Germany," 2021. [Online]. Available: https://www.ise.fraunhofer.de/en/publications/studies/recent-facts-about-pv-in-germany.html

[11] H. Baker, *Alloy Phase Diagrams: ASM Handbook,* 3rd ed.: ASM International, 1992.

[12] DERA and BGR, "Preismonitor September 2022," [Online]. Available: https://www.deutsche-rohstoffagentur.de/DERA/DE/Aktuelles/Monitore/2022/09-22/2022-09-preismonitor.pdf?__blob=publicationFile&v=2

[13] J. R. Rumble, *CRC handbook of chemistry and physics,* 98th ed. Boca Raton, Florida: CRC Press, 2017. [Online]. Available: http://hbcponline.com/

[14] S. Zhou, C. Yang, Y.-A. Shen, S. Lin, and H. Nishikawa, "The newly developed Sn–Bi–Zn alloy with a low melting point, improved ductility, and high ultimate tensile strength," *Materialia*, vol. 6, p. 100300, 2019, doi: 10.1016/j.mtla.2019.100300.

[15] D. C. Adriano, *Trace Elements in Terrestrial Environments: Biogeochemistry, Bioavailability, and Risks of Metals,* 2nd ed.: Springer New York, 2001.

[16] D. L. King, M. A. Quintana, J. A. Kratochvil, D. E. Ellibee, and B. R. Hansen, "Photovoltaic module performance and durability following long-term field exposure," (in English), *Prog. Photovolt: Res. Appl.*, vol. 8, no. 2, pp. 241–256, 2000.

[17] J.-S. Jeong, N. Park, and C. Han, "Field failure mechanism study of solder interconnection for crystalline silicon photovoltaic module," *Microelectronics Reliability*, vol. 52, 9-10, pp. 2326–2330, 2012, doi: 10.1016/j.microrel.2012.06.027.

[18] *DIN 8580:2003-09, Fertigungsverfahren_-Begriffe, Einteilung,* DIN Deutsches Institut für Normung e. V. (DIN), Berlin, 2003.

[19] M. Schaefer, R. A. Fournelle, and J. Liang, "Theory for intermetallic phase growth between cu and liquid Sn-Pb solder based on grain boundary diffusion control," (in English), *Journal of Elec Materi*, vol. 27, no. 11, pp. 1167–1176, 1998, doi: 10.1007/s11664-998-0066-7.

[20] T. An and F. Qin, "Effects of the intermetallic compound microstructure on the tensile behavior of Sn3.0Ag0.5Cu/Cu solder joint under various strain rates," *ELTE 2010 & IMAPS/CPMT Poland 2010*, vol. 54, no. 5, pp. 932–938, 2014, doi: 10.1016/j.microrel.2014.01.008.

[21] T. Geipel, M. Moeller, A. Kraft, and U. Eitner, "A comprehensive study of intermetallic compounds in solar cell interconnections and their growth kinetics," *Enrgy Proced*, vol. 98, pp. 86–97, 2016.

[22] P. Schmitt, P. Kaiser, C. Savio, M. Tranitz, and U. Eitner, "Intermetallic phase growth and reliability of Sn-Ag-soldered solar cell joints," *Enrgy Proced*, vol. 27, pp. 664–669, 2012, doi: 10.1016/j.egypro.2012.07.126.

[23] Y.-J. Jeon, M.-S. Kang, and Y.-E. Shin, "Growth of an Ag3Sn Intermetallic Compound Layer Within Photovoltaic Module Ribbon Solder Joints," *Int. J. of Precis. Eng. and Manuf.-Green Tech.*, vol. 7, no. 1, pp. 89–96, 2020, doi: 10.1007/s40684-019-00028-1.

[24] H. Gopalakrishna *et al.,* "Activation Energy for End-of-Life Solder Bond Degradation: Thermal Cycling of Field-Aged PV Modules," *IEEE Journal of Photovoltaics*, vol. 10, no. 6, pp. 1762–1771, 2020, doi: 10.1109/JPHOTOV.2020.3025726.

[25] P. L. Tu, Y. Chan, and J. Lai, "Effect of intermetallic compounds on the thermal fatigue of surface mount solder joints," *IEEE Trans. Compon. Packag. Manuf. Technol. B*, vol. 20, no. 1, pp. 87–93, 1997, doi: 10.1109/96.554534.

[26] D. R. Frear and P. T. Vianco, "Intermetallic growth and mechanical behavior of low and high melting temperature solder alloys," *Metall and Mat Trans A*, vol. 25, no. 7, pp. 1509–1523, 1994, doi: 10.1007/BF02665483.

[27] G. Zeng, S. Xue, L. Zhang, L. Gao, W. Dai, and J. Luo, "A review on the interfacial intermetallic compounds between Sn–Ag–Cu based solders and substrates," *Journal of Materials Science: Materials in Electronics*, vol. 21, no. 5, pp. 421–440, 2010, doi: 10.1007/s10854-010-0086-y.

[28] M. H. Poech, "Schädigungsmechanismen in Lötverbindungen bei erhöhter Temperatur," *Verfahrenstechnik der Energiewandlung (VTE)*, vol. 14, no. 1, pp. 12–18, 2002.

[29] R. J. Borg and G. J. Dienes, *An Introduction to Solid State Diffusion*. San Diego: Academic Press, 1988.

[30] H. L. Harald Ibach, *Solid-State Physics: An Introduction to Principles of Materials Science,* 4th ed. Berlin, Heidelberg: Springer Berlin Heidelberg, 2009.

[31] *Umgebungseinflüsse - Teil 2-2: Prüfverfahren - Prüfung B: Trockene Wärme*, DIN EN 60068-2-2, Deutsches Institut für Normung e.V. (DIN), 2008.

[32] *DIN EN ISO 14577-1:2015-11, Metallische Werkstoffe_- Instrumentierte Eindringprüfung zur Bestimmung der Härte und anderer Werkstoffparameter_- Teil_1: Prüfverfahren (ISO_14577-1:2015); Deutsche Fassung EN_ISO_14577-1:2015*, Berlin.

[33] D. Hull and D. J. Bacon, *Introduction to Dislocations,* 5th ed.: Elsevier, 2011.

[34] G. Gottstein, *Materialwissenschaft und Werkstofftechnik,* 4th ed.: Springer-Verlag, 2014.

[35] J. A. Marqusee and J. Ross, "Theory of Ostwald ripening: Competitive growth and its dependence on volume fraction," *The Journal of Chemical Physics*, vol. 80, no. 1, pp. 536–543, 1984, doi: 10.1063/1.446427.

[36] J. Rösler, H. Harders, and M. Bäker, *Mechanisches Verhalten der Werkstoffe,* 4th ed. Wiesbaden: Springer Fachmedien Wiesbaden, 2012.

[37] P. G. Harris, K. S. Chaggar, and M. A. Whitmore, "The effect of ageing on the microstructure of 60:40 tin-lead solders," *Soldering & Surface Mount Tech*, vol. 3, no. 1, pp. 20–33, 1991, doi: 10.1108/eb037741.

[38] H. Ma and J. C. Suhling, "A review of mechanical properties of lead-free solders for electronic packaging," *J Mater Sci*, vol. 44, no. 5, pp. 1141–1158, 2009, doi: 10.1007/s10853-008-3125-9.

[39] Y. Tian, W. Liu, R. An, W. Zhang, L. Niu, and C. Wang, "Effect of intermetallic compounds on fracture behaviors of Sn3.0Ag0.5Cu lead-free solder joints during in situ tensile test," *J Mater Sci: Mater Electron*, vol. 23, no. 1, pp. 136–147, 2012, doi: 10.1007/s10854-011-0538-z.

[40] M. A. Quintana, D. L. King, T. J. McMahon, and C. R. Osterwald, "Commonly observed degradation in field-aged photovoltaic modules," in *Proceedings of the 29th IEEE Photovoltaic Specialists Conference*, New Orleans, Louisiana, USA, 2002, pp. 1436–1439.

[41] U. Itoh, M. Yoshida, H. Tokuhisa, K. Takeuchi, and Y. Takemura, "Solder joint failure modes in the conventional crystalline Si module," *Energy Procedia*, vol. 55, pp. 464–468, 2014.

[42] G. Cuddalorepatta, A. Dasgupta, S. Sealing, J. Moyer, and Tolliver, T.Loman, J., "Durability of Pb-free solder between copper interconnect and silicon in photovoltaic cells," *Prog. Photovolt: Res. Appl.*, vol. 18, no. 3, pp. 168–182, 2010, doi: 10.1002/pip.944.

[43] *Terrestrial photovoltaic (PV) modules – Design qualification and type approval – Part 1-3: Special requirements for testing of thin-film amorphous silicon based photovoltaic (PV) modules*, IEC 61215-1-3:2016, International Electrotechnical Commission (IEC), Geneva, Switzerland, 2016.

[44] Deutscher Wetterdienst, "Klimastatusbericht Deutschland Jahr 2022," Geschäftsbereich Klima und Umwelt, Offenbach, 2022. [Online]. Available: www.dwd.de/DE/derdwd/bibliothek/fachpublikationen/selbstverlag/selbstverlag_node.html

[45] T. An and F. Qin, "Relationship Between the Intermetallic Compounds Growth and the Microcracking Behavior of Lead-Free Solder Joints," *J. Electron. Packag.*, vol. 138, no. 1, 2016, doi: 10.1115/1.4032349.